ACS NANO

www.acsnano.org

ARTICLE

Increased Nanoparticle Delivery to Brain Tumors by Autocatalytic Priming for Improved Treatment and Imaging

Liang Han,[†] Derek K. Kong,[†] Ming-qiang Zheng,[‡] Sasidhar Murikinati,[§] Chao Ma,[†] Peng Yuan,[§] Liyuan Li,[†] Daofeng Tian,[†] Qiang Cai,[†] Chunlin Ye,[†] Daniel Holden,[‡] June-Hee Park,[§] Xiaobin Gao,[⊥] Jean-Leon Thomas,[§] Jaime Grutzendler,[§] Richard E. Carson,[‡] Yiyun Huang,[‡] Joseph M. Piepmeier,[†] and Jiangbing Zhou*[,†,#]

[†]Department of Neurosurgery, [#]Department of Biomedical Engineering, [‡]PET Center, Department of Diagnostic Radiology, [§]Department of Neurology, and [⊥]Department of Pathology, Yale University, New Haven, Connecticut 06511, United States

Supporting Information

ABSTRACT: **The blood–brain barrier (BBB) is partially disrupted in brain tumors. Despite the gaps in the BBB, there is an inadequate amount of pharmacological agents delivered into the brain. Thus, the low delivery efficiency renders many of these agents ineffective in treating brain cancer. In this report, we proposed an "autocatalytic" approach for increasing the transport of nanoparticles into the brain. In this strategy, a small number of nanoparticles enter into the brain *via* transcytosis or through the BBB gaps. After penetrating the BBB, the nanoparticles release BBB modulators, which enables more nanoparticles to be transported, creating a positive feedback loop for increased delivery. Specifically, we demonstrated that these autocatalytic brain tumor-targeting poly(amine-*co*-ester) terpolymer nanoparticles (ABTT NPs) can readily cross the BBB and preferentially accumulate in brain tumors at a concentration of 4.3- and 94.0-fold greater than that in the liver and in brain regions without tumors, respectively. We further demonstrated that ABTT NPs were capable of mediating brain cancer gene therapy and chemotherapy. Our results suggest ABTT NPs can prime the brain to increase the systemic delivery of therapeutics for treating brain malignancies.**

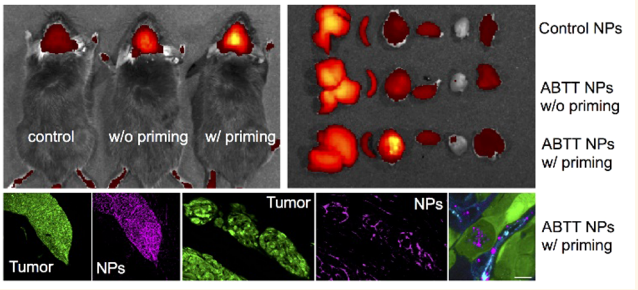

KEYWORDS: *autocatalytic delivery, blood–brain barrier, brain cancer, nanoparticles*

Brain cancer is a devastating disease. The worldwide incidence of brain cancer, including primary brain cancer and brain metastases, was 256 000 in 2012.[1] Despite surgical and medical advances, the prognosis for most brain cancer patients remains dismal. The median survival for glioblastoma (the most common malignant glioma in adults),[2] diffuse intrinsic pontine glioma (the most common type of brainstem glioma in children),[3] and brain metastasis[4] is 14, 9, and 12 months, respectively. Novel therapeutic approaches with improved efficacy for these tumors are urgently needed.

Improved pharmacological treatment of brain cancer has been limited by the lack of delivery platforms that are able to efficiently overcome the blood–brain barrier (BBB). Although local BBB disruption is observed in large brain tumors, these "leaky" blood vessels are located primarily in the tumor center, whereas the capillaries feeding the proliferating tumor edge remain impermeable.[5] The BBB can potentially be bypassed using invasive methods, such as surgical implantation of degradable Gliadel wafers or locoregional administration of poly(lactic-*co*-glycolic acid) (PLGA) brain-penetrating nanoparticles (NPs).[6,7] Unfortunately, the clinical utility of these approaches is hampered by these tumors' highly invasive nature. In addition, restricted drug penetration to distant tumor cells that are separate from the tumor bulk limits their therapeutic efficacy.[8,9]

Nanotechnology represents a promising approach for the intravenous delivery of therapeutic agents to the brain.[10−12] The primary advantage of nanotechnology is that NPs can be engineered to exploit many mechanisms for brain-targeted delivery, including (1) receptor-mediated transcytosis (RMT);[13] (2) carrier-mediated transcytosis (CMT);[14] (3) adsorptive-mediated transcytosis (AMT);[15] and (4) disease microenvironment-targeted delivery.[16] Despite these advantages, nanotechnology for systemic gene delivery to the brain is still in its

Received: December 1, 2015
Accepted: March 11, 2016
Published: March 11, 2016

DOI: 10.1021/acsnano.5b07573
ACS Nano 2016, 10, 4209–4218

infancy. Existing engineering approaches often fail to enhance systemic delivery of NPs to the brain to a degree sufficient for treatment purposes.[10−12] It was recently reported that gold NPs can be engineered to cross the BBB and deliver siRNA to brain tumors, providing a survival benefit of several days in mice. However, these inorganic NPs are incapable of carrying large pieces of genetic material and providing protection against nuclease degradation.[17] There is, however, evidence that nonpolymeric NPs may be modified for diagnostic purposes, such as iron oxide-containing NPs, which can facilitate imaging of brain tumors.[16]

To overcome this challenge, we propose an autocatalytic brain tumor-targeting (ABTT) delivery strategy (Figure 1). With this

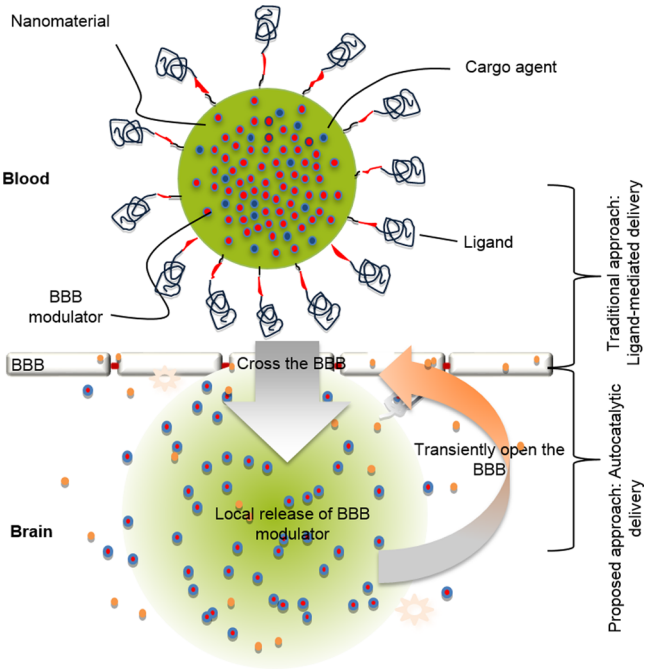

Figure 1. Schematic of autocatalytic delivery of brain tumor-targeted NPs.

delivery method, a small fraction of NPs enter the brain tumor microenvironment through a traditional mechanism, either RMT, CMT, AMT, or disease-targeted delivery, in addition to BBB leakage. After reaching tumors, NPs locally release BBB modulators, which in turn transiently enhance BBB permeability to allow additional NPs to enter the same region. Through this secondary autocatalysis mechanism, the delivery procedure creates a positive feedback loop. As a result, the efficiency of NP accumulation in tumors autocatalytically increases with time and subsequent administrations.

In this study, we tested this strategy by synthesizing ABTT NPs using a biodegradable poly(amine-*co*-ester) terpolymer. The traditional delivery approach was achieved *via* a disease microenvironment-targeted mechanism through surface conjugation of chlorotoxin (CTX), a 36-amino acid peptide with high affinity for matrix metalloproteinase-2 (MMP2), which is preferentially up-regulated in brain tumors but not in the normal brain.[18] Autocatalysis was achieved though encapsulation of Lexiscan, a small molecule known to have the ability to transiently enhance BBB permeability.[19] We demonstrated that the resulting ABTT NPs were capable of penetrating the BBB in tumors with high efficiency and mediated effective brain cancer gene therapy and chemotherapy.

RESULTS AND DISCUSSION

We recently developed enzyme-catalyzed chemistry for polymerization of diethyl sebacate (DES) and *N*-methyldiethanolamine (MDEA) with lactones.[20] The chemistry allows fine-tuning of four features in a single polymer molecule: density of positive charge, molecular weight, hydrophobicity, and crystallinity.[20,21] In our previous report, we studied a group of liquid terpolymers synthesized through this chemistry and found that many of them were capable of forming liquid polyplex NPs for efficient gene delivery.[20] However, due to the limited stability and drug-loading capacity, these liquid polyplex NPs are not suitable for systemic drug delivery to the brain (data not shown). To overcome these limitations, we tuned the chemistry by incorporating a high content (40−80%) of hydrophobic lactones and synthesized a family of solid terpolymers (Figure S1A, Table S1). We screened these polymers and selected 62%-HDL-DES-MDEA (III-62%), which contains 38% DES/MDEA and 62% hexadecanolide (HDL) in moles and is capable of forming spherical NPs with a low polydispersity index (Figure S1B,C, Table S2). III-62% was further modified to display maleimide groups on the NP surface (Figure S2). With this chemistry, we synthesized III-62% NPs with surface conjugation of mHph2 and found that the resulting mHph2-III-62% NPs were able to deliver genes with efficiency greater than polyethylenimine (PEI) and Lipofectamine 2000 (Figure S3). mHph2, which has the amino acid sequence YARVRRRGPRRHHHHHHHHHC, a modified mHph1 peptide, with amino acid sequence CHHHHHYA-RVRRRGPRRHHHHHC, is a cell penetration peptide that we previously developed for enhancing gene delivery efficiency.[22] Different from mHph1, mHph2 contains a single cysteine and thus allows precise control of conjugation through cysteine-maleimide reaction. Compared to PEI, mHph2-III-62% NPs exhibited lower cell toxicity *in vitro* (Figure S4).

We examined mHph2-III-62% NPs for systemic drug delivery to brain tumors using mice bearing intracranial GL261 gliomas, a mouse model that has previously been shown to have a compromised BBB comparable to that in human glioblastoma multiforme (GBM).[23−25] NPs were synthesized with encapsulation of IR780, a near-infrared fluorescent dye that allows for noninvasive detection using an IVIS imaging system. We found that mHph2-III-62% NPs had limited ability to penetrate the BBB in tumors but that further conjugation with CTX enhanced the delivery by 1.9-fold (Figure S5). Nonetheless, despite the enhancement, the accumulation of NPs in brain tumors was significantly lower than that in the liver, suggesting that traditional engineering approaches may be inadequate to overcome the BBB.[26,27]

Synthesis and Characterization of ABTT NPs. To further enhance systemic drug delivery to brain tumors, we proposed incorporating a secondary, autocatalytic drug delivery mechanism through encapsulation of a BBB modulator (Figure 1). We evaluated three well-characterized BBB modulators: Lexiscan,[19] NECA [1-(6-amino-9*H*-purin-9-yl)-1-deoxy-*N*-ethyl-β-D-ribofuranuronamide],[19] and minoxidil.[28] NECA and Lexiscan are adenosine receptor agonists that enhance BBB permeability by decreasing transendothelial electrical resistance, increasing actinomyosin stress fiber formation, and altering tight junction molecules.[19] Minoxidil is a selective K_{ATP} channel agonist that increases the permeability of the BBB in tumors by down-regulating tight junction protein expression.[29] To enable

DOI: 10.1021/acsnano.5b07573
ACS Nano 2016, 10, 4209−4218

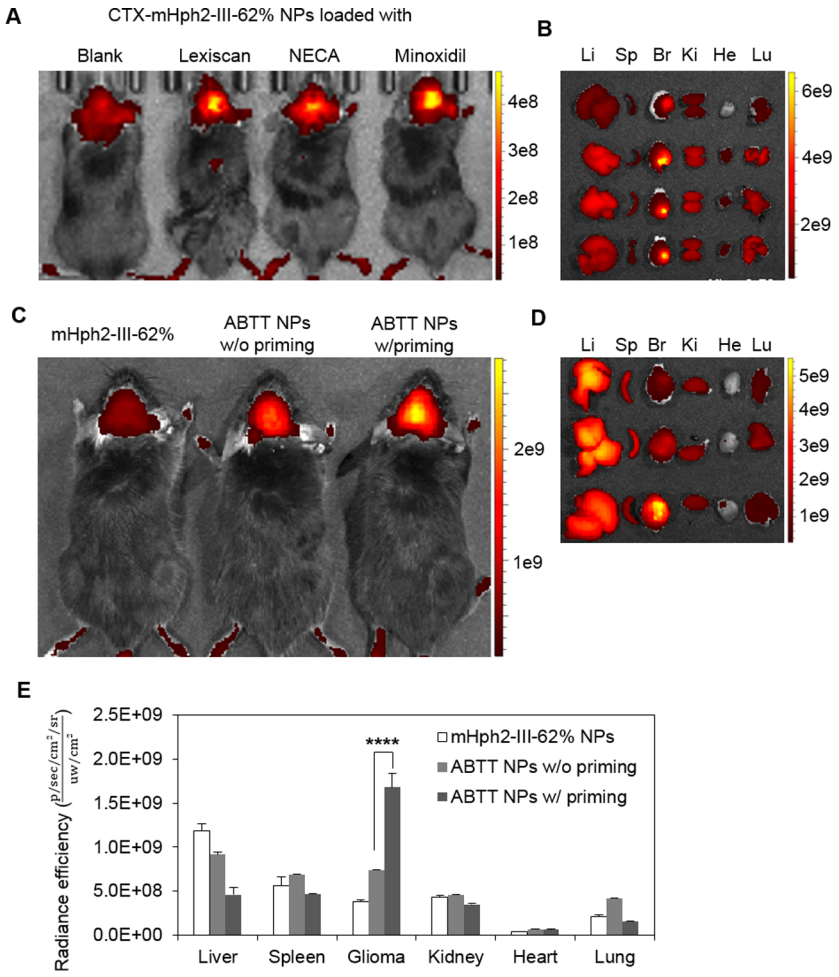

Figure 2. Synthesis and evaluation of ABTT NPs. (A, B) Encapsulation of BBB modulators for enhanced drug delivery to brain tumors. Three BBB modulators, Lexiscan, NECA, and minoxidil, were loaded into CTX-mHph2-III-62% NPs and intravenously administered to GL261 tumor-bearing mice. Fluorescence signals in mice (A) and excised organs (B) were registered at 24 h after the last NP treatment using an IVIS imaging system. Panels in B from top to bottom represent CTX-mHph2-III-62% NPs without any BBB modulator and with Lexiscan, NECA, and minoxidil, respectively. Li, Sp, Br, Ki, He, and Lu represent liver, spleen, brain, kidney, heart, and lung, respectively. (C−E) Brain tumor-targeting efficacy of ABTT NPs increased with time and subsequent administrations. After receiving two intravenous administrations of unlabeled CTX-mHph2-III-62% NPs (w/o priming) or ABTT NPs (w/priming), mice received treatment of IR780-loaded ABTT NPs. One day later, fluorescence signals in mice (C) and excised organs (D) were determined using an IVIS imaging system. Mice treated with IR780-labeled mHph2-III-62% NPs were used as controls. Panels in D from top to bottom represent mHph2-III-62% NPs, ABTT NPs w/o priming, and ABTT NPs w/priming, respectively. Unit for color bars: radiance efficiency $\left(\frac{\mathrm{p/s/cm^2/sr}}{\mathrm{uw/cm^2}}\right)$. (E) Semiquantification of NPs in indicated organs based on fluorescence intensity. The radiance efficiency on the *y*-axis was determined using Living Image 3.0 by dividing the fluorescence signal intensity with area of region of interest, which is tumor size in this study. All experiments were carried out in triplicate, and the standard deviation is denoted using error bars. ** represents $p < 0.0001$ for comparison of tumor accumulation between ABTT NPs with priming and ABTT NPs without priming.**

autocatalytic delivery, mice bearing GL261 tumors received a single tail vein injection daily of NPs coloaded with IR780 and BBB modulator for three consecutive days. Twenty-four hours after the last injection, both live mice and excised organs were imaged using an IVIS imaging system. As shown in Figure 2A,B, Lexiscan, NECA, and minoxidil significantly enhanced delivery of CTX-mHph2-III-62% NPs to the brain with comparable efficiency. The signal intensity of NPs in the tumor-bearing right brain surpassed that in all other organs including the liver, kidney, spleen, heart, and lung. Of the three BBB modulators, Lexiscan is currently used in the clinic in an intravenous formulation for myocardial perfusion imaging and has a favorable safety profile. Therefore, Lexiscan was selected for further studies. The Lexiscan loading was 1.1%. Encapsulation of Lexiscan did not change the morphology of CTX-mHph2-III-62% NPs (Figure S6A) or their ability to transfect cells (Figure S6B). Lexiscan was released from the NPs in a controlled manner (Figure S6C). In accordance with our proposed mechanism, we found that the tumor accumulation efficiency autocatalytically increased with subsequent administrations: the efficiency was enhanced by 2.26-fold simply by priming mice with two treatments of the same NPs without IR780 (Figure 2C−E). With this delivery strategy, the signal intensity of NPs in the brain tumor was 4.3, 4.2, 5.6, 31.7, and 12.7 times greater than that in the liver, spleen, kidney, heart, and lung, compared to 0.3, 0.7, 0.9, 9.6, and 1.8 times for mHph2-III-62% NPs (Figure 2E). These results were likely due to the combinatorial effect of tumor targeting by CTX and autocatalysis by Lexiscan (Figure S6D). To further simplify the nomenclature,

DOI: 10.1021/acsnano.5b07573
ACS Nano 2016, 10, 4209−4218

we designated CTX-mHph2-III-62% NPs loaded with Lexiscan as ABTT NPs. Tables S2−S5 summarize the characteristics of ABTT NPs used in this study. ABTT NPs were synthesized with high reproducibility (Table S5). Liver function evaluation by alanine amino transferase (ALT) and aspartate amino transferase (AST) assays suggested that ABTT NPs had limited *in vivo* toxicity (Figure S7).

ABTT NPs for Systemic Delivery of Brain Cancer Imaging. We next evaluated the ability to enhance the imaging of brain tumors. We labeled ABTT NPs and control mHph2-III-62% NPs with a radioactive tag by reacting the free amine group on the NPs with *N*-succinimidyl 4-[^{18}F]-fluorobenzoate (SFB) to form an amide bond (4-[^{18}F]-fluorobenzamide-NPs) (Figure S8). We then administered the labeled NPs to GL261 tumor-bearing mice through tail vein injection after first priming with three injections of unlabeled NPs. Approximately 20 min after administration, positron emission tomography/computed tomography (PET/CT) scans were performed under anesthesia. The accumulation of NPs in the brain was continuously monitored for 4 h. Resulting images were reconstructed (OSEM) with corrections for decay, randoms, attenuation, and scatter. The left and right brain regions of interest in the PET images were manually drawn based on merged PET/CT images. Results in Figure 3A, which showed the summed PET image (210−240 min), demonstrate the dynamic increase in PET signal, suggesting that ABTT NPs penetrated the BBB and accumulated in tumors. In comparison, control mHph2-III-62% NPs demonstrated much lower efficiency. We quantified the radioactivity within the tumor and the corresponding left hemisphere based on mean pixel values, which were converted to standard uptake values (SUVs, activity normalized to dose per body weight). We found that the radioactivity within the tumor continuously increased over the entire 4 h period. In contrast, the radioactivity within the corresponding left hemisphere remained low over this time window (Figure 3B). On the basis of a separate study in which the kinetics of NP accumulation in brain tumors were measured based on the IR780 signal, we found that the accumulation of NPs in brain tumors peaked between 8 and 12 h post-treatment (Figure S9A,B). The PET signals and IR780 signals detected in tumors likely originated from NPs. In the PET study, the radiotracer was conjugated to NPs *via* stable covalent amide bonds and thus was unlikely to be detached from NPs in the experimental time window. In the fluorescence study, IR780 could not be efficiently released from NPs due to its high hydrophobicity (Figure S9C). Therefore, within the experimental window, the majority of IR780 remained in NPs.

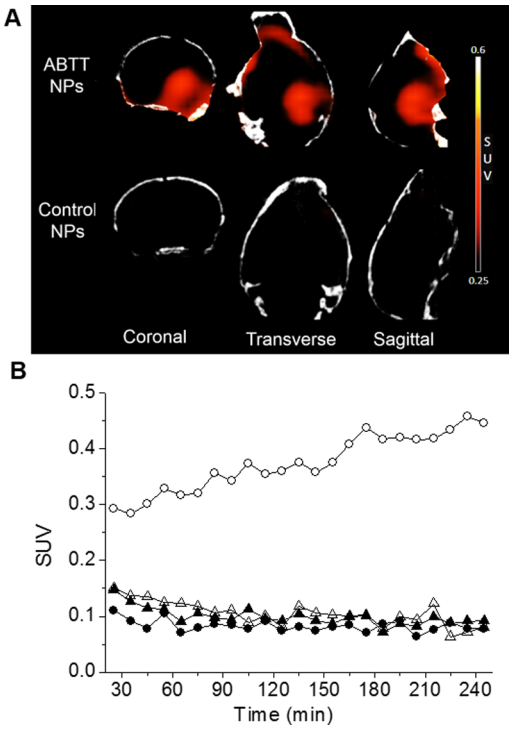

Figure 3. PET imaging of ABTT NPs in brain tumors. (A) Summed PET images of ^{18}F-labeled ABTT (top row) and control NPs (bottom row) merged with CT images in a brain tumor mouse model. Only SUVs larger than 0.25 were shown. The evaluation was performed in duplicate. Data from a representative pair of mice (mouse treated with ABTT NPs and mouse treated with control NPs) are presented. (B) Dynamic change in radioactivity with time in tumor (right brain) and corresponding left hemisphere without tumors. Open circles and solid circles represent the right brain and the left brain, respectively, of a mouse that received ABTT NPs. Open triangle and solid triangle represent the right brain and the left brain, respectively, of a mouse that received control NPs.

To further characterize the penetrability of ABTT NPs into the brain at the cellular level, we examined the location of ABTT NPs in the brain using high-resolution confocal microscopy. In this study, we treated mice bearing green fluorescent protein (GFP)-expressing tumor with ABTT NPs encapsulating DiD, a red fluorescence dye, after which, mice were euthanized and extensively perfused. The brains were sectioned and subjected to microscopic analysis. Consistent with previous findings, we found that ABTT NPs (magenta) preferentially accumulated in intracranial tumors (green) and were distributed over the entire brain tumor region; in contrast, a limited amount of NPs accumulated in the surrounding normal brain tissue (Figure 4A−C, Figure S10A−E). The fluorescence intensity in the tumors as determined by ImageJ was 94.0 times greater than that in nontumor regions of the same brains (Figure 4D). This difference may reflect the difference in NP concentration in the tumor and nontumor regions, as the fluorescence intensity is linearly correlated with NP concentration (Figure S10F). We found a fraction of ABTT NPs located perivascularly around tumor blood vessels (cyan), suggesting that they crossed the BBB in the tumors (Figure 4E). With further magnification, we detected a cluster of NPs located within a single cell, suggesting that ABTT NPs were capable of penetrating cell membranes and entering cellular compartments with high efficiency (Figure 4F). Notably, in addition to tremendous specificity, ABTT NPs also demonstrated high sensitivity for tumor cells, as they were able to efficiently accumulate in small distant tumor islands that contained only 10−20 tumor cells (Figure 4G−I).

ABTT NPs have limited ability to penetrate the normal brain. We administered IR780-loaded ABTT NPs to mice without tumors, which were primed with unlabeled ABTT NP treatments twice. IR780-loaded ABTT NPs were undetectable in the normal brain (Figure S11). We further examined the penetrability of ABTT NPs, using confocal microscopy, in the brain of VEGFR3-YFP transgenic mice, in which the endothelial cells of blood vessels, radial glia cells, and neural stem cells are labeled with yellow fluorescent protein (YFP). We found that, except in the circumventricular organs, which are known to lack a restrictive BBB, all other regions of the brain had minimal accumulation of particles (Figure S12). Through these studies, we demonstrate that ABTT NPs are highly specific for tumors in the brain but exhibit minimal accumulation in normal brain tissue.

DOI: 10.1021/acsnano.5b07573
ACS Nano 2016, 10, 4209−4218

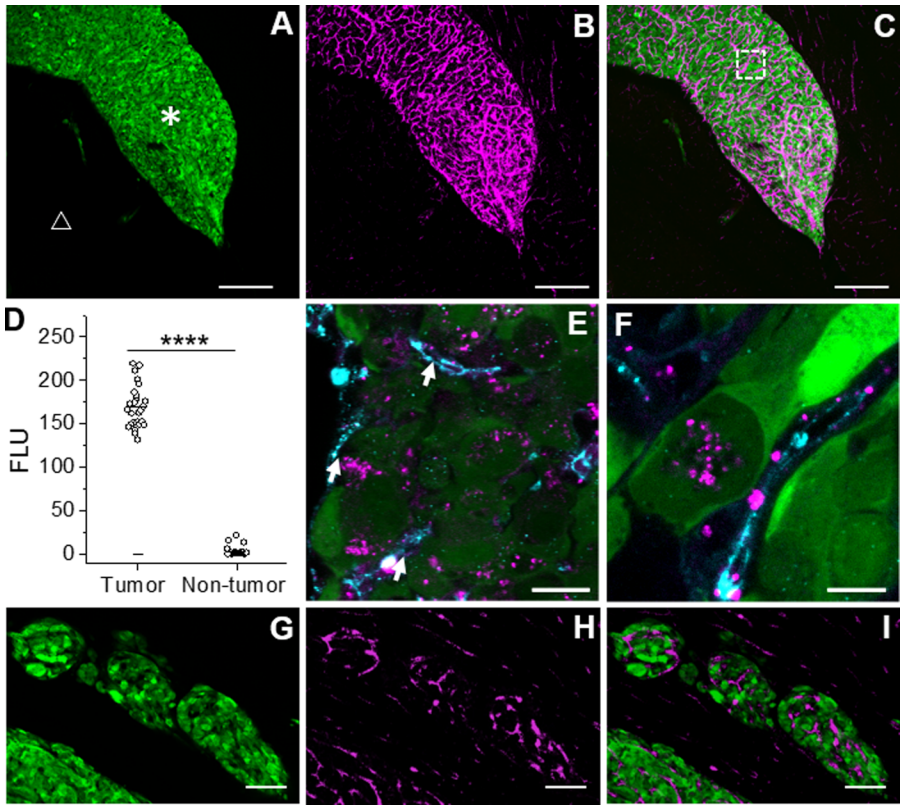

Figure 4. Imaging of ABTT NPs in the mouse brain using confocal microscopy. (A–C) ABTT NPs (magenta) demonstrated specific binding to the tumor (green) with almost no binding to tumor-free regions. * and Δ mark regions with and without tumors, respectively. (D) Fluorescence intensities (FLU) of DiD in tumor and nontumor regions. The ratio of average FLU in tumors to that in nontumor regions was 94.0 (169.6 *vs* 1.8). Fluorescence intensity was quantified using ImageJ (NIH). Data were acquired from three mice. ** represents $p < 0.0001$. (E) Magnified image of the merged image of tumor (green) and NPs (magenta) along with the PECAM vessel labeling (cyan), demonstrating effective crossing of the vascular–tumor barrier. (F) ABTT NPs (magenta) crossed the vascular barrier (cyan) and were engulfed by the tumor cells (green). (G–I) ABTT NPs (magenta) effectively binding to small tumor islands (green) adjacent to a larger tumor lobule, with little binding outside the islands. Scale bar: (A–C) 100 μm; (E) 10 μm; (F) 5 μm; (G–I) 20 μm.**

ABTT NPs for Systemic Delivery of Brain Cancer Gene Therapy. To assess the ability of ABTT NPs to transfect brain cancer cells, we treated GL261 cells with luciferase plasmid-encapsulated ABTT NPs, which retained their spherical morphology at 161 nm (Figure 5A). By using the expression of the luciferase gene as a reporter, ABTT NPs transfected GL261 cells with an efficiency significantly greater than that of Lipofectamine 2000. At 72 h, the luciferase signal in ABTT NP-treated cells was 48.1 times greater than that in Lipofectamine 2000-treated cells (Figure 5B). Intravenous administration of pRFP-loaded ABTT NPs efficiently transfected GL261 tumors in the brain, as evident by the strong red fluorescent signal in tumors and limited signal in normal brain tissue and nontransfected tumors (Figure S13A). Finally, we evaluated ABTT NPs for systemic delivery of gene therapy to GL261 gliomas. Malignant gliomas often evolve a variety of mechanisms to reduce the expression of B7-1, a costimulatory molecule necessary for T-lymphocyte activation.[30] Correspondingly, cytotoxic T-lymphocytes fail to recognize and eradicate the tumors.[31,32] Therefore, one potential approach to treat malignant gliomas is to restore the normal function of B7-1 by delivering the B7-1 gene directly to tumors. To test this approach and evaluate the use of ABTT NPs for systemic delivery of gene therapy, we administered B7-1 plasmid DNA (pB7-1)-loaded ABTT NPs to intracranial GL261 tumor-bearing mice through tail vein injection and monitored their survival over time. pB7-1-loaded ABTT NPs were spherical in morphology with an average diameter of 157 nm and showed minimal cytotoxicity to GL261 cells (Figure S13B,C). Kaplan–Meier analysis revealed that mice treated with B7-1 gene-loaded ABTT NPs had significant improvement in median survival, which was 38 days, compared to 28 and 29 days for mice receiving saline and blank ABTT NPs, respectively (Figure 5C, $p < 0.0001$ for both comparisons). Successful delivery of pB7-1 was confirmed by B7-1 immunostaining (Figure 5D). In contrast to blank ABTT-NP-treated tumors, the B7-1-loaded ABTT NP-treated tumors showed significant up-regulation of B7-1. The efficacy of pB7-1 gene-loaded ABTT NPs was limited to 10-day survival enhancement, presumably owing to an intrinsic limitation of the GL261 intracranial tumor model. T-cells cannot enter the brain unless they are activated. Apparently, intracranial inoculation of GL261 cells does not allow for penetration of an adequate number of T-lymphocytes, as a single intratumoral administration of pB7-1-loaded ABTT NPs eliminated tumors implanted in the flank (Figure S13D).

We further evaluated ABTT NPs for systemic gene therapy in U87-MG-derived human glioma. Consistent with our findings in the GL261 model, intravenous administration of ABTT NPs results in preferential accumulation of NPs in tumors with high efficiency (Figure S14). When pRFP was encapsulated, ABTT NPs selectively transfected intracranial tumors (Figure S15A,B). Intravenous administration of plasmid expressing tumor necrosis

DOI: 10.1021/acsnano.5b07573
ACS Nano 2016, 10, 4209–4218

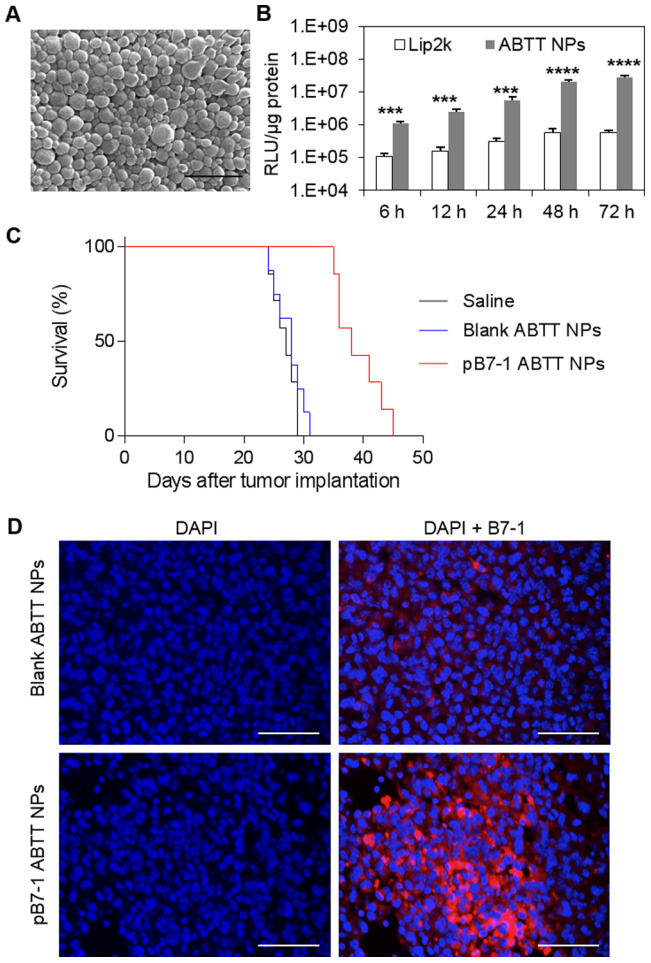

Figure 5. ABTT NPs for systemic delivery of gene therapy to brain cancer. (A) Representative SEM image of DNA-loaded ABTT NPs. Scale bar represents 500 nm. (B) Gene delivery efficiency of pGL4.13-loaded ABTT NPs (filled bar) and Lipofectamine 2000 (Lip2k, open bar) on GL261 glioma cells. Experiments were carried out in triplicate, and the standard deviation is denoted using error bars. Luciferase signal was detected at 6, 12, 24, 48, and 72 h after transfection and normalized to the amount of total protein for comparison. * and **** represent $p < 0.001$ and 0.0001, respectively. (C) Kaplan–Meier survival curves for intracranial GL261 tumor-bearing mice with indicated treatments: red line, pB7-1-loaded ABTT NPs (median survival 38 d); blue line, blank ABTT NPs (median survival 28 d); black line, saline treatment (median survival 27 d). Each group contained 8 mice. (D) Expression of B7-1 in tumors. Scale bar represents 100 μm.**

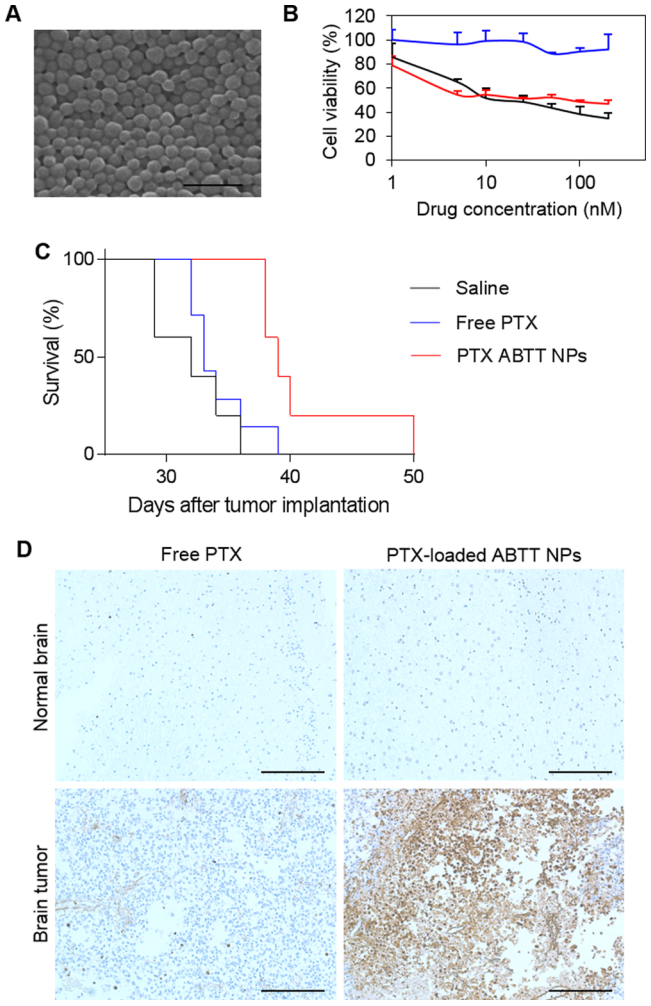

Figure 6. ABTT NPs for systemic delivery of chemotherapy for brain cancer. (A) Representative SEM image of PTX-loaded ABTT NPs. Scale bar represents 500 nm. (B) Toxicity of PTX-loaded ABTT NPs (red line), blank ABTT NPs (black line), and free PTX (blue line) on GL261 cells. All experiments were carried out in triplicate, and the standard deviation is denoted using error bars. (C) Kaplan–Meier survival curves for intracranial GL261 tumor-bearing mice with indicated treatments: red line, PTX-loaded ABTT NPs (median survival 39 d); blue line, free PTX (median survival 33 d); black line, saline treatment (median survival 32 d). Each group included 8 mice. (D) TUNEL staining demonstrated significant tumor apoptosis in mice treated with PTX-loaded ABTT NPs. Scale bar represents 100 μm.

factor-related apoptosis-inducing ligand (pTRAIL)-loaded ABTT NPs significantly enhanced tumor-bearing mouse survival (Figure S15C). In particular, 2 of 6 mice in the treatment group survived over 90 days, and tumors in the brains of these mice were undetectable by luciferase imaging (Figure S15D).

ABTT NPs for Systemic Delivery of Brain Cancer Chemotherapy. We next assessed the use of ABTT NPs for systemic delivery of chemotherapy to brain cancer. Paclitaxel (PTX), a drug previously shown to inhibit GL261 cells,[33] was selected as a model drug. PTX was encapsulated into ABTT NPs with an efficiency of 15% by weight. PTX-loaded ABTT NPs had spherical morphology and a diameter of 112 nm (Figure 6A) and had toxicity to GL261 cells comparable to that of free drug (Figure 6B). Intravenous treatment with the PTX-loaded ABTT NPs enhanced the median survival of tumor-bearing mice, which was 39 days, compared to 32 and 33 days for mice receiving saline and free PTX, respectively ($p < 0.05$) (Figure 6C). TUNEL staining revealed a significant increase in the number of apoptotic cells after treatment with PTX-loaded ABTT NPs (Figure 6D).

We next evaluated PTX-loaded ABTT NPs for systemic treatment of MDA-MB-231-BR-HER2 brain metastases of breast cancer.[34,35] Different from the GL261 model, which forms a single tumor mass in the brain, the MDA-MB-231-BR-HER2 brain metastases of the breast cancer model produce many tumor lesions throughout the brain, thus representing one of the most challenging brain tumor models for brain cancer chemotherapy.[36,37] We confirmed that intravenous administration of ABTT NPs resulted in efficient NP accumulation in tumor lesions (Figure S16A,B). We administered the PTX-encapsulated ABTT NPs to mice with MDA-MB-231-BR-HER2 brain

DOI: 10.1021/acsnano.5b07573
ACS Nano 2016, 10, 4209–4218

metastases of breast cancer and monitored their survival over time. PTX-loaded ABTT NPs significantly enhanced tumor-bearing mouse survival: The median survival time for mice receiving PTX-loaded ABTT NPs was 63 days. This was significantly longer than that for mice receiving either saline (39 days), blank ABTT NPs (43 days), or free PTX (45 days) (Figure S16C, $p < 0.05$ for both comparisons). In accordance with this finding, mice treated with blank ABTT NPs had many large lesions in the brain at day 35, whereas the mice that received treatment of PTX-loaded ABTT NPs had only one single small lesion (Figure S16D).

Of note, in both gene therapy and chemotherapy studies, mice received 9 treatments of NPs at a dose of 2 mg/injection (50 nmol/injection). The maximum tolerable dose for ABTT NPs is greater than 10 mg/injection (250 nmol/injection). Therefore, it is likely that further enhanced therapeutic benefit can be achieved with more aggressive treatment regimens.

CONCLUSION AND OUTLOOK

In this study, we proposed an autocatalytic strategy to improve the delivery of brain tumor-targeting solid poly(amine-*co*-ester) terpolymer NPs. The terpolymer III-62% was selected, as it has the capacity for efficient drug loading and gene delivery. Solid polymeric NPs have advantages over many other vehicles when used for gene delivery in terms of protecting encapsulated genetic materials from nuclease degradation. Compared to gene delivery using certain inorganic NPs, such as gold NPs, in which genetic materials are conjugated to their surface and thus directly exposed to nucleases, the solid polymeric NPs encapsulate cargo in a polymer matrix, which physically shields genetic materials from nuclease degradation. Compared to complex-based NPs, such as lipoplexes or polyplexes, which typically are unstable in complex biological environments, the solid polymeric NPs have a stable structure to enable effective protection of cargo DNA or RNA in the circulatory system. As expected, terpolymer NPs without further engineering had limited ability to penetrate the BBB in brain tumors. We found that NPs engineered through the traditional disease microenvironment-targeted mechanism *via* CTX enhanced the delivery by 2-fold, a degree of enhancement consistent with previous reports.[16] When further engineered through the autocatalytic mechanism that we proposed, the resulting ABTT NPs efficiently overcame the BBB in all three tested brain cancer models, including the GL261 murine glioma model, the U87 human GBM model, and the MDA-MB-231-BR-HER2 brain metastasis model, resulting in an efficient approach for systemic delivery of both chemotherapy and gene therapy to brain cancer. In addition to chemotherapy and gene therapy, ABTT NPs may also be engineered for brain cancer diagnosis, as our PET imaging and high-resolution confocal microscopy studies demonstrated that ABTT NPs were able to identify brain tumors including small satellite tumor islands containing a limited number of tumor cells. Such great sensitivity may be clinically useful in the diagnosis and treatment of small satellite tumor islands, which are not amenable to surgical resection and are often responsible for patient relapse and death. ABTT NPs exhibited less cytotoxicity than the commercial transfection agent PEI *in vitro* (Figure S4) and demonstrated a favorable safety profile for *in vivo* use, as determined by the liver function ALT and AST tests (Figure S7). In the PET imaging study, we used the radiotracer ^{18}F for NP labeling and observed strong specific signal accumulation in the brain (Figure 3A). The observed signal was not due to free ^{18}F, as unconjugated ^{18}F is known to have high affinity for bone[38] and limited ability to penetrate the BBB.[39] Therefore, the PET signal detected is attributed to ^{18}F conjugated to the surface of ABTT NPs. These observations suggested that ABTT NPs are stable in the systemic circulation. This stability is further supported by the observation of NPs in brain tumors (Figure 4E,F) and by an *in vitro* serum stability assay (Figure S17).

We are aware of the limitations of this study. Lexiscan has been reported to enhance BBB permeability in the literature.[19,40,41] In these reports, Lexiscan was administered intravenously. In this situation, Lexiscan modulates BBB permeability likely through interaction with adenosine A2A receptor expressed on the luminal side of the BBB. In the present study, ABTT NPs containing Lexiscan remain intact in the circulatory system. Therefore, the BBB modulation effect of ABTT NPs is likely due to Lexiscan released from the brain parenchyma. The mechanism of how Lexiscan modulates BBB permeability from the abluminal side of the endothelium has not been elucidated. The abluminal side of the BBB consists of endothelial cells surrounded by astrocytes, pericytes, and neurons, and the permeability of the BBB is tightly regulated by astrocytes and pericytes.[42−44] The A2A Lexiscan receptor is expressed in brain endothelial cells,[19,45,46] astrocytes,[47] pericytes,[48] and neurons,[49] and administration of A2A modulators from the abluminal side of the brain significantly affected brain capillary dilatation and blood flow through interaction with a variety of cells.[50−52] Therefore, it is possible that Lexiscan exerts its biological activity through interaction with one or more of these cell types. However, we cannot exclude the possibility that Lexiscan modulates BBB permeability primarily through interaction with brain endothelial cells. In this case, we need to determine whether A2A is expressed on both the apical and basal aspects of endothelial cells. To support this hypothesis, researchers have examined cell cultures that showed the expression of A2A in brain endothelial cells is not polarized.[19,45,46] The physiological evidence, which was described in this article as well as in the literature,[50−52] also suggests that A2A is expressed on both the apical and basolateral aspects of the cell rather than one or the other. However, conclusive characterization of apical and basal expression of A2A requires imaging A2A *in situ* in brain slides using quantitative immune-electron microscopy, and further mechanistic studies are needed.

Due to their unprecedented efficiency in crossing the BBB, their great capacity to accommodate and deliver cargo agents, and their construction from biodegradable materials with reasonable toxicity, we anticipate that ABTT NPs can be useful for the clinical management of brain cancer. Further enhancement of ABTT NP delivery efficiency could be potentially achieved through engineering ABTT NPs to trigger drug release in the brain tumor microenvironment, such as incorporation of acid-sensitive moieties into polymers.

MATERIALS AND METHODS

Synthesis of ABTT NPs. Polymers used in this study were synthesized according to procedures described in the Supporting Information. ABTT NPs were synthesized according to a standard emulsion procedure.[6,7,22] Briefly, for the synthesis of DNA-loaded NPs, 500 μg of DNA in 100 μL of water was added dropwise to 100 mg of mIII-62% (2.5 μmol) in 2 mL of dichloromethane (DCM) containing 2.5 mg of Lexiscan (6.4 μmol) under vortex. This mixture was sonicated to form a water/oil emulsion (first emulation). The water/oil emulsion was then added dropwise to 4 mL of 2.5% PVA under vortex and sonicated to form a water/oil/water emulsion (second emulation). The double emulsion was poured into a beaker containing 0.3% PVA and stirred for 3 h to evaporate DCM. NPs were collected by centrifugation

DOI: 10.1021/acsnano.5b07573
ACS Nano 2016, 10, 4209−4218

at 20 000 rpm for 30 min. The precipitate was suspended in phosphate buffer saline (PBS) and reacted first with thiolated CTX (32 μg, 8 nmol) for 1 h at room temperature and then with excess cysteine-terminated peptide mHph2 (4 mg, 0.8 μmol) for 1 h at room temperature. The unreacted CTX and mHph2 were removed by centrifugation at 20 000 rpm for 30 min, and the precipitate was suspended in H_2O and lyophilized for storage and characterization. For synthesis of IR780-, DiD-, or PTX-loaded NPs, the same procedures without the first emulation step were used. Physical characteristics of ABTT NPs used in this study are summarized in Tables S3−S5.

Tumor Models. All procedures were approved by the Institutional Animal Care and Utilization Committee (IACUC) of Yale University. Mice were purchased from Charles River Laboratories. To establish intracranial GL261 mouse xenografts, 5−6-week-old female C57BL6 mice were anesthetized *via* intraperitoneal injection of ketamine and xylazine. Twenty-thousand GL261 cells in 2 μL of PBS were injected into the right striatum 2 mm lateral and 0.5 mm posterior to the bregma and 3 mm below the dura using a stereotactic apparatus with an UltraMicroPump (UMP3) (World Precision Instruments, FL, USA). The U87-MG mouse model was established according to the same procedures except that nude mice were used. The brain metastasis model was established according to previously reported methods with minor modifications.[34,35,53] Briefly, 5−6-week-old female nude mice were anesthetized and firmly secured with front paws extended above the head. About 250 000 MDA-MB-231-BR-HER2 cells in 0.1 mL of PBS were loaded into a syringe with a 26-G needle. After inserting the needle into the second intercostal space 3 mm to the left of the sternum with a depth of ∼6 mm, cells were injected slowly over 20−30 s. The GL261 flank tumor model was established through injection of 1×10^6 GL261 cells in 100 μL of PBS subcutaneously into the right flank region of female C57BL6 mice.

PET Imaging Procedures and Imaging Analysis. PET scan and image analysis were carried out using a microPET scanner (Inveon, Siemens Medical Solutions). All preprimed brain tumor model mice (4 experimental animals and 4 controls) were injected intravenously with ∼0.5 mCi (0.2 mL) of [^{18}F]-labeled ABTT NPs or mHph2-III-62% NPs while awake. A pair of mice was then lightly anesthetized and placed on the microPET scanner to first receive a short CT scan. Dynamic PET scans were then acquired over 4 h. PET images were reconstructed using a two-dimensional ordered-subset expectation maximum (OSEM) algorithm with no correction for attenuation or scatter. The left and right brain regions of interest in the PET images were manually drawn based on the merged PET/CT image. Radioactivity within the tumor and the corresponding left hemisphere were obtained from mean pixel values within the multiple region of interest volume and then converted to MBq/mL and standardized to percent injected dose per gram (%ID/g).

High-Resolution Confocal Microscopy Study of ABTT NPs in Brain Tumors. Mice containing gliomas received four ABTT NP injections. Two days after NP injections, 100 μL of PE rat anti-mouse CD31 antibody (BD Pharmingen #553373) was injected intravenously to label the tumor vasculature. One hour after injecting the antibody, mice were perfused with 1× PBS followed by 4% paraformaldehyde (PFA). Brains were incubated overnight in 4% PFA, and 60 μm thick sections were obtained using a vibratome (Leica). Tumor-containing brain sections were mounted and used for high-resolution confocal imaging. A Leica SP5 confocal microscope with 10× air, 40×, and 63× objectives with APO oil immersion was used to obtain Z-stacks at 0.5 μm step sizes and zooms from 1 to 5. Images were processed using NIH ImageJ.

Therapeutic Evaluation and Histological Assessment. For evaluation in subcutaneous GL261 tumors, treatments were started when tumor volumes reached ∼50 mm.[3] Tumor size was measured two times a week using traceable digital vernier calipers (Fisher). The tumor volumes were determined by measuring the length (l) and the width (w) and calculating the volume ($V = 1/2 \times lw^2$). For intracranial tumors, treatments were started 5 days after the tumor cell injection. Injections were performed through the tail vein 3 days a week for 3 weeks at a dose of 2 mg NPs/mouse/injection (50 nmol/injection). The animals' weight, grooming, and general health were monitored on a daily basis. Mice were euthanized after either a 15% loss in body weight or when it was humanely necessary due to clinical symptoms. The animals were sacrificed 2 days after the last treatment, whereupon the brains were excised and formalin fixed for immunohistochemistry. To detect B7-1 expression within the pB7-1-loaded ABTT NPs-treated intracranial GL261 tumors, sectioned brains were stained with anti-CD80 antibody labeled with Alexa Fluor 647. To analyze the therapeutic effects of PTX-loaded ABTT NPs, slides of serial brain sections were stained with terminal deoxynucleotidyl transferase (TUNEL) for analysis of therapeutic effects.

Statistical Analysis. All data were collected in triplicate and reported as mean and standard deviation. Comparison of two conditions was evaluated by the unpaired t test. One-way ANOVA analysis was performed to determine the statistical significance of treatment-related changes in survival. $p < 0.05$ (*), 0.01 (**), 0.001 (***), and 0.0001 (****) were considered significant.

ASSOCIATED CONTENT

Supporting Information

The Supporting Information is available free of charge on the ACS Publications website at DOI: 10.1021/acsnano.5b07573.

Supporting results, materials, and methods (PDF)

AUTHOR INFORMATION

Corresponding Author

*E-mail: jiangbing.zhou@yale.edu.

Author Contributions

J.Z. and L.H. designed the experiments. L.H., D.K., M.Z., S.M., C.M., P.Y., Q.C., L.L., D.T., C.Y., D.H., and J.-H.P. performed the experiments. All the authors were involved in the analyses and interpretation of data. J.Z., L.H., and D.K. wrote the paper, with the help of the coauthors.

Notes

The authors declare no competing financial interest.

ACKNOWLEDGMENTS

The authors thank Dr. Z. Jiang for assistance with polymer characterization, Dr. K. Lim for providing the radiolabeling precursor for the [^{18}F]SFB, and J. Ropchan, T. Mulnix, and K. Fowles for their professional assistance in the PET imaging. This work was supported by NIH Grants CTSA UL1 TR000142 and NS095817, the Matthew Larson Foundation, and the State of Connecticut. This research was partially supported by scholarships from the Chinese Scholarship Council to Q.C., D.T., C.M., and C.Y.

REFERENCES

(1) Ferlay, J.; Soerjomataram, I.; Ervik, M. *Globocan 2012 V1. 0, Cancer Incidence and Mortality Worldwide*; Iarc Cancer Base No. 10 [Internet]; International Agency for Research on Cancer: Lyon, 2013.

(2) Scott, C. B.; Scarantino, C.; Urtasun, R.; Movsas, B.; Jones, C. U.; Simpson, J. R.; Fischbach, A. J.; Curran, W. J., Jr. Validation and Predictive Power of Radiation Therapy Oncology Group (Rtog) Recursive Partitioning Analysis Classes for Malignant Glioma Patients: A Report Using Rtog 90−06. *Int. J. Radiat. Oncol., Biol., Phys.* **1998**, *40*, 51−55.

(3) Khatua, S.; Moore, K. R.; Vats, T. S.; Kestle, J. R. W. Diffuse Intrinsic Pontine Glioma-Current Status and Future Strategies. *Childs Nerv. Syst.* **2011**, *27*, 1391−1397.

(4) Jaboin, J. J.; Ferraro, D. J.; Dewees, T. A.; Rich, K. M.; Chicoine, M. R.; Dowling, J. L.; Mansur, D. B.; Drzymala, R. E.; Simpson, J. R.; Magnuson, W. J. Survival Following Gamma Knife Radiosurgery for Brain Metastasis from Breast Cancer. *Radiat. Oncol.* **2013**, *8*, 1−8.

(5) Blakeley, J. Drug Delivery to Brain Tumors. *Curr. Neurol. Neurosci. Rep.* **2008**, *8*, 235−241.

DOI: 10.1021/acsnano.5b07573
ACS Nano 2016, 10, 4209−4218

(6) Strohbehn, G.; Coman, D.; Han, L.; Ragheb, R. R.; Fahmy, T. M.; Huttner, A. J.; Hyder, F.; Piepmeier, J. M.; Saltzman, W. M.; Zhou, J. Imaging the Delivery of Brain-Penetrating PLGA Nanoparticles in the Brain Using Magnetic Resonance. *J. Neuro-Oncol.* **2015**, *121*, 441−449.
(7) Zhou, J.; Patel, T. R.; Sirianni, R. W.; Strohbehn, G.; Zheng, M.-Q.; Duong, N.; Schafbauer, T.; Huttner, A. J.; Huang, Y.; Carson, R. E.; Zhang, Y.; Sullivan, D. J., Jr.; Piepmeier, J. M.; Saltzman, W. M. Highly Penetrative, Drug-Loaded Nanocarriers Improve Treatment of Glioblastoma. *Proc. Natl. Acad. Sci. U. S. A.* **2013**, *110*, 11751−11756.
(8) Fung, L. K.; Shin, M.; Tyler, B.; Brem, H.; Saltzman, W. M. Chemotherapeutic Drugs Released from Polymers: Distribution of 1,3-Bis(2-Chloroethyl)-1-Nitrosourea in the Rat Brain. *Pharm. Res.* **1996**, *13*, 671−682.
(9) Fung, L. K.; Ewend, M. G.; Sills, A.; Sipos, E. P.; Thompson, R.; Watts, M.; Colvin, O. M.; Brem, H.; Saltzman, W. M. Pharmacokinetics of Interstitial Delivery of Carmustine, 4-Hydroperoxycyclophosphamide, and Paclitaxel from a Biodegradable Polymer Implant in the Monkey Brain. *Cancer Res.* **1998**, *58*, 672−684.
(10) Deeken, J. F.; Loscher, W. The Blood-Brain Barrier and Cancer: Transporters, Treatment, and Trojan Horses. *Clin. Cancer Res.* **2007**, *13*, 1663−1674.
(11) Patel, T.; Zhou, J.; Piepmeier, J. M.; Saltzman, W. M. Polymeric Nanoparticles for Drug Delivery to the Central Nervous System. *Adv. Drug Delivery Rev.* **2012**, *64*, 701−705.
(12) Zhou, J.; Atsina, K. B.; Himes, B. T.; Strohbehn, G. W.; Saltzman, W. M. Novel Delivery Strategies for Glioblastoma. *Cancer J.* **2012**, *18*, 89−99.
(13) Qiao, R.; Jia, Q.; Huwel, S.; Xia, R.; Liu, T.; Gao, F.; Galla, H. J.; Gao, M. Receptor-Mediated Delivery of Magnetic Nanoparticles across the Blood-Brain Barrier. *ACS Nano* **2012**, *6*, 3304−3310.
(14) Li, J.; Guo, Y.; Kuang, Y.; An, S.; Ma, H.; Jiang, C. Choline Transporter-Targeting and Co-Delivery System for Glioma Therapy. *Biomaterials* **2013**, *34*, 9142−9148.
(15) Liu, L.; Venkatraman, S. S.; Yang, Y. Y.; Guo, K.; Lu, J.; He, B.; Moochhala, S.; Kan, L. Polymeric Micelles Anchored with Tat for Delivery of Antibiotics across the Blood-Brain Barrier. *Biopolymers* **2008**, *90*, 617−623.
(16) Veiseh, O.; Sun, C.; Fang, C.; Bhattarai, N.; Gunn, J.; Kievit, F.; Du, K.; Pullar, B.; Lee, D.; Ellenbogen, R. G.; Olson, J.; Zhang, M. Q. Specific Targeting of Brain Tumors with an Optical/Magnetic Resonance Imaging Nanoprobe across the Blood-Brain Barrier. *Cancer Res.* **2009**, *69*, 6200−6207.
(17) Jensen, S. A.; Day, E. S.; Ko, C. H.; Hurley, L. A.; Luciano, J. P.; Kouri, F. M.; Merkel, T. J.; Luthi, A. J.; Patel, P. C.; Cutler, J. I. Spherical Nucleic Acid Nanoparticle Conjugates as an Rnai-Based Therapy for Glioblastoma. *Sci. Transl. Med.* **2013**, *5*, 2124−2134.
(18) Deshane, J.; Garner, C. C.; Sontheimer, H. Chlorotoxin Inhibits Glioma Cell Invasion Via Matrix Metalloproteinase-2. *J. Biol. Chem.* **2003**, *278*, 4135−4144.
(19) Carman, A. J.; Mills, J. H.; Krenz, A.; Kim, D. G.; Bynoe, M. S. Adenosine Receptor Signaling Modulates Permeability of the Blood-Brain Barrier. *J. Neurosci.* **2011**, *31*, 13272−13280.
(20) Zhou, J.; Liu, J.; Cheng, C. J.; Patel, T. R.; Weller, C. E.; Piepmeier, J. M.; Jiang, Z.; Saltzman, W. M. Biodegradable Poly(Amine-Co-Ester) Terpolymers for Targeted Gene Delivery. *Nat. Mater.* **2012**, *11*, 82−90.
(21) Voevodina, I.; Scandola, M.; Zhang, J. W.; Jiang, Z. Z. Exploring the Solid State Properties of Enzymatic Poly(Amine-Co-Ester) Terpolymers to Expand Their Applications in Gene Transfection. *RSC Adv.* **2014**, *4*, 8953−8961.
(22) Zhou, J.; Patel, T. R.; Fu, M.; Bertram, J. P.; Saltzman, W. M. Octa-Functional Plga Nanoparticles for Targeted and Efficient Sirna Delivery to Tumors. *Biomaterials* **2012**, *33*, 583−591.
(23) Yung, R.; Seyfoddin, V.; Guise, C.; Tijono, S.; McGregor, A.; Connor, B.; Ching, L. M. Efficacy against Subcutaneous or Intracranial Murine Gl261 Gliomas in Relation to the Concentration of the Vascular-Disrupting Agent, 5,6-Dimethylxanthenone-4-Acetic Acid (Dmxaa), in the Brain and Plasma. *Cancer Chemother. Pharmacol.* **2014**, *73*, 639−649.
(24) Leten, C.; Struys, T.; Dresselaers, T.; Himmelreich, U. In Vivo and Ex Vivo Assessment of the Blood Brain Barrier Integrity in Different Glioblastoma Animal Models. *J. Neuro-Oncol.* **2014**, *119*, 297−306.
(25) Becker, C. M.; Oberoi, R. K.; Mcfarren, S. J.; Muldoon, D. M.; Pafundi, D. H.; Pokorny, J. L.; Brinkmann, D. H.; Ohlfest, J. R.; Sarkaria, J. N.; Largaespada, D. A. Decreased Affinity for Efflux Transporters Increases Brain Penetrance and Molecular Targeting of a Pi3k/Mtor Inhibitor in a Mouse Model of Glioblastoma. *Neuro. Oncol.* **2015**, *17*, 1210.
(26) Huang, R.; Han, L.; Li, J.; Liu, S.; Shao, K.; Kuang, Y.; Hu, X.; Wang, X.; Lei, H.; Jiang, C. Chlorotoxin-Modified Macromolecular Contrast Agent for Mri Tumor Diagnosis. *Biomaterials* **2011**, *32*, 5177−5186.
(27) Huang, R.; Ke, W.; Han, L.; Li, J.; Liu, S.; Jiang, C. Targeted Delivery of Chlorotoxin-Modified DNA-Loaded Nanoparticles to Glioma Via Intravenous Administration. *Biomaterials* **2011**, *32*, 2399−2406.
(28) Ningaraj, N. S.; Rao, M. K.; Black, K. L. Adenosine 5′-Triphosphate-Sensitive Potassium Channel-Mediated Blood-Brain Tumor Barrier Permeability Increase in a Rat Brain Tumor Model. *Cancer Res.* **2003**, *63*, 8899−8911.
(29) Gu, Y.-t.; Xue, Y.-x.; Wang, Y.-f.; Wang, J.-h.; Chen, X.; ShangGuan, Q.-r.; Lian, Y.; Zhong, L.; Meng, Y.-n. Minoxidil Sulfate Induced the Increase in Blood−Brain Tumor Barrier Permeability through Ros/Rhoa/Pi3k/Pkb Signaling Pathway. *Neuropharmacology* **2013**, *75*, 407−415.
(30) Chen, L.; Flies, D. B. Molecular Mechanisms of T Cell Co-Stimulation and Co-Inhibition. *Nat. Rev. Immunol.* **2013**, *13*, 227−242.
(31) Han, S. J.; Zygourakis, C.; Lim, M.; Parsa, A. T. Immunotherapy for Glioma: Promises and Challenges. *Neurosurg. Clin. N. Am.* **2012**, *23*, 357−370.
(32) Capece, D.; Verzella, D.; Fischietti, M.; Zazzeroni, F.; Alesse, E. Targeting Costimulatory Molecules to Improve Antitumor Immunity. *J. Biomed. Biotechnol.* **2012**, *2012*, 926321.
(33) Passarella, R. J.; Spratt, D. E.; van der Ende, A. E.; Phillips, J. G.; Wu, H.; Sathiyakumar, V.; Zhou, L.; Hallahan, D. E.; Harth, E.; Diaz, R. Targeted Nanoparticles That Deliver a Sustained, Specific Release of Paclitaxel to Irradiated Tumors. *Cancer Res.* **2010**, *70*, 4550−4559.
(34) Palmieri, D.; Bronder, J. L.; Herring, J. M.; Yoneda, T.; Weil, R. J.; Stark, A. M.; Kurek, R.; Vega-Valle, E.; Feigenbaum, L.; Halverson, D.; Vortmeyer, A. O.; Steinberg, S. M.; Aldape, K.; Steeg, P. S. Her-2 Overexpression Increases the Metastatic Outgrowth of Breast Cancer Cells in the Brain. *Cancer Res.* **2007**, *67*, 4190−4198.
(35) Yoneda, T.; Williams, P. J.; Hiraga, T.; Niewolna, M.; Nishimura, R. A Bone-Seeking Clone Exhibits Different Biological Properties from the Mda-Mb-231 Parental Human Breast Cancer Cells and a Brain-Seeking Clone in Vivo and in Vitro. *J. Bone Miner. Res.* **2001**, *16*, 1486−1495.
(36) Lockman, P. R.; Mittapalli, R. K.; Taskar, K. S.; Rudraraju, V.; Gril, B.; Bohn, K. A.; Adkins, C. E.; Roberts, A.; Thorsheim, H. R.; Gaasch, J. A.; Huang, S.; Palmieri, D.; Steeg, P. S.; Smith, Q. R. Heterogeneous Blood-Tumor Barrier Permeability Determines Drug Efficacy in Experimental Brain Metastases of Breast Cancer. *Clin. Cancer Res.* **2010**, *16*, 5664−5678.
(37) Mittapalli, R. K.; Liu, X. L.; Adkins, C. E.; Nounou, M. I.; Bohn, K. A.; Terrell, T. B.; Qhattal, H. S.; Geldenhuys, W. J.; Palmieri, D.; Steeg, P. S.; Smith, Q. R.; Lockman, P. R. Paclitaxel-Hyaluronic Nanoconjugates Prolong Overall Survival in a Preclinical Brain Metastases of Breast Cancer Model. *Mol. Cancer Ther.* **2013**, *12*, 2389−2399.
(38) Czernin, J.; Satyamurthy, N.; Schiepers, C. Molecular Mechanisms of Bone 18f-Naf Deposition. *J. Nucl. Med.* **2010**, *51*, 1826−1829.
(39) Guerrero, S.; Herance, J. R.; Rojas, S.; Mena, J. F.; Gispert, J. D.; Acosta, G. A.; Albericio, F.; Kogan, M. J. Synthesis and in Vivo Evaluation of the Biodistribution of a 18f-Labeled Conjugate Gold-Nanoparticle-Peptide with Potential Biomedical Application. *Bioconjugate Chem.* **2012**, *23*, 399−408.
(40) Gao, X.; Qian, J.; Zheng, S.; Changyi, Y.; Zhang, J.; Ju, S.; Zhu, J.; Cong, L. Overcoming the Blood-Brain Barrier for Delivering Drugs into

DOI: 10.1021/acsnano.5b07573
ACS Nano 2016, 10, 4209−4218

the Brain by Using Adenosine Receptor Nanoagonist. *ACS Nano* **2014**, *8*, 3678−3689.
(41) Zheng, S.; Bai, Y. Y.; Liu, Y.; Gao, X.; Yan, L.; Changyi, Y.; Wang, Y.; Di, C.; Ju, S.; Cong, L. Salvaging Brain Ischemia by Increasing Neuroprotectant Uptake Via Nanoagonist Mediated Blood Brain Barrier Permeability Enhancement. *Biomaterials* **2015**, *66*, 9−20.
(42) Winkler, E. A.; Bell, R. D.; Zlokovic, B. V. Central Nervous System Pericytes in Health and Disease. *Nat. Neurosci.* **2011**, *14*, 1398−1405.
(43) Neuwelt, E. A.; Bauer, B.; Fahlke, C.; Fricker, G.; Iadecola, C.; Janigro, D.; Leybaert, L.; Molnar, Z.; O'Donnell, M. E.; Povlishock, J. T.; Saunders, N. R.; Sharp, F.; Stanimirovic, D.; Watts, R. J.; Drewes, L. R. Engaging Neuroscience to Advance Translational Research in Brain Barrier Biology. *Nat. Rev. Neurosci.* **2011**, *12*, 169−182.
(44) Abbott, N. J.; Ronnback, L.; Hansson, E. Astrocyte-Endothelial Interactions at the Blood-Brain Barrier. *Nat. Rev. Neurosci.* **2006**, *7*, 41−53.
(45) Mills, J. H.; Alabanza, L.; Weksler, B. B.; Couraud, P. O.; Romero, I. A.; Bynoe, M. S. Human Brain Endothelial Cells Are Responsive to Adenosine Receptor Activation. *Purinergic Signalling* **2011**, *7*, 265−273.
(46) Bynoe, M. S.; Viret, C.; Yan, A.; Kim, D. G. Adenosine Receptor Signaling: A Key to Opening the Blood−Brain Door. *Fluids Barriers CNS* **2015**, *12*, 1−12.
(47) Matos, M.; Augusto, E.; Agostinho, P.; Cunha, R. A.; Chen, J. F. Antagonistic Interaction between Adenosine A2a Receptors and Na+/K+-Atpase-Alpha2 Controlling Glutamate Uptake in Astrocytes. *J. Neurosci.* **2013**, *33*, 18492−18502.
(48) Li, Q.; Puro, D. G. Adenosine Activates Atp-Sensitive K(+) Currents in Pericytes of Rat Retinal Microvessels: Role of A1 and A2a Receptors. *Brain Res.* **2001**, *907*, 93−99.
(49) Kaster, M. P.; Machado, N. J.; Silva, H. B.; Nunes, A.; Ardais, A. P.; Santana, M.; Baqi, Y.; Muller, C. E.; Rodrigues, A. L. S.; Porciuncula, L. O.; Chen, J. F.; Tome, A. R.; Agostinho, P.; Canas, P. M.; Cunha, R. A. Caffeine Acts through Neuronal Adenosine A2a Receptors to Prevent Mood and Memory Dysfunction Triggered by Chronic Stress. *Proc. Natl. Acad. Sci. U. S. A.* **2015**, *112*, 7833−7838.
(50) Hirao, M.; Oku, H.; Goto, W.; Sugiyama, T.; Kobayashi, T.; Ikeda, T. Effects of Adenosine on Optic Nerve Head Circulation in Rabbits. *Exp. Eye Res.* **2004**, *79*, 729−735.
(51) Gordon, G. R.; Howarth, C.; MacVicar, B. A. Bidirectional Control of Arteriole Diameter by Astrocytes. *Exp. Physiol.* **2011**, *96*, 393−399.
(52) Phillis, J. W.; O'Regan, M. H. Effects of Adenosine Receptor Antagonists on Pial Arteriolar Dilation During Carbon Dioxide Inhalation. *Eur. J. Pharmacol.* **2003**, *476*, 211−219.
(53) Kang, Y. Analysis of Cancer Stem Cell Metastasis in Xenograft Animal Models. *Methods Mol. Biol.* **2009**, *568*, 7−19.

DOI: 10.1021/acsnano.5b07573
ACS Nano 2016, 10, 4209−4218